Eqs. (13) and (19), respectively. To the order of terms to be retained here, they are found to be

$$A_1 = 0 \tag{24a}$$

$$C_i = \frac{1}{2(1+\gamma)} \tag{24b}$$

Using the asymptotic solutions thus obtained and the surface condition, Eq. (12), as the boundary conditions for $D \to \infty$ and at $D = 0$, respectively, the differential equation, Eq. (23), is now integrated to obtain the nondimensional distribution function Φ. It is then introduced into the integrals, Eqs. (9), to determine the flow properties N, U, and P (or Θ), where we expand them into a series of functions, $J_n(D)$, ($n = 1, 2, 3, \ldots$), defined as

$$J_n(D) = \int_0^\infty x^n \exp\left(-x^2 - \frac{x}{D}\right) dx \tag{25}$$

All of the coefficients contained in the flow properties may be determined numerically by applying the moment method,[3] i.e., multiplying both sides of Eqs. (9) by $D^l (l = 0, 1, 2, \ldots)$ and integrating them with respect to D from $D = 0$ to ∞ gives rise to simultaneous linear equations for those constants.

Drag of a Liquid Sphere

As a final solution, the drag of a liquid sphere is determined by integrating the momentum flux[3] over the entire sphere surface and found to be

$$D = D_s\left(1 - \frac{2}{3} C_i - \frac{2}{3} KB_1\right) \tag{26}$$

where D_s is the conventional Stokes drag given by

$$D_s = 6\pi\mu u_\infty a \tag{27}$$

Figure 2 shows dependence of the drag ratio D/D_s on γ with K as a parameter. In this figure, increasing values of γ indicate that effects of the internal circulation decrease and that the flow behavior essentially approaches that for a solid sphere. In the case of $K = 0$, which implies the continuum flow, the drag ratio is somewhat smaller than unity for small values of γ, suggesting the effect of the internal circulation. The drag ratio then approaches unity as the value of γ increases. For other values of K, the rarefaction of the external flow effectively diminishes the drag ratio, which is interpreted as the effect of the velocity slip at the sphere surface. This rarefaction effect is more pronounced for larger values of γ as indicated in the case of $K = 0.7$.

Conclusions

The kinetic theory analysis was carried out to investigate the slow flow of rarefied gas past a liquid spherical drop. The linearized BGKW model of the Boltzmann equation was employed to solve the flow outside the sphere, and the analysis was extended to the first order of the Knudsen number. The circulating internal flow of liquid within the sphere was also analyzed. As a result, it was found that the significant internal circulation would occur when the viscosity of the external gas and that of the internal liquid are comparable to each other in magnitude. This results in reduction of the sphere drag from the conventional Stokes drag. The rarefaction of the external flow also has a decreasing effect on the drag by the order of the Knudsen number, which is greater for larger values of the viscosity ratio between the internal liquid and the external gas.

References

[1]Bhatnagar, P. L., Gross, E. P., and Krook, M., "A Model for Collision Processes in Charged and Neutral One-Component Systems," *Physical Review*, Vol. 94, No. 3, 1954, pp. 511-525.

[2]Welander, P., "On the Temperature Jump in a Rarefied Gas," *Arkiv for Physik*, Vol. 7, No. 44, 1954, pp. 507-553.

[3]Tomoeda, M., "A Theoretical and Experimental Study on the Flow of Rarefied Gas Past a Sphere," Univ. of Toronto Inst. for Aerospace Studies, UTIAS Rept. 216, Toronto, Ontario, Canada, May 1977.

Comparison of Chemical Kinetic Rate Mechanisms for High-Temperature Air, Including Electronic Energy

Yvette Weber* and John Anderson Jr.†
University of Maryland,
College Park, Maryland 20742

Introduction

THE purpose of this work is to examine and compare the behavior of several chemical kinetic models in high-temperature air that are currently popular for modern high-temperature flowfield analyses and also to examine the effect of simultaneously assuming a finite equilibrium electronic energy. For this investigation a sample gas dynamic model is used, namely, the inviscid, nonequilibrium chemically reacting flowfield downstream of a normal shock wave in air. This flow is calculated using both the Dunn and Kang and the Park kinetic mechanisms. Local thermodynamic equilibrium is assumed in all calculations. Comparisons are made between results obtained from both models along with results obtained from a hybrid model that applies Gupta's curve fits for the equilibrium constants of the reactions. Calculations are performed with and without the inclusion of equilibrium electronic energy as part of the mixture enthalpy. Results show that, although the different kinetic models tend toward the same equilibrium condition far downstream, the rates of chemical relaxation can vary widely between models. Also, the addition of the electronic energy is shown to produce only small changes in the flowfield properties and species mass fractions.

Contents

Over the past several years there has been much interest in the design of high Mach number, high-altitude vehicles such as the aeroassisted space transfer vehicle (ASTV). Under these conditions, it is likely that the flowfield will be in local chemical and thermal nonequilibrium and that a significant portion of the heat transfer will come from radiative nonequilibrium.[1] Since these nonequilibrium processes affect the performance of the vehicle, it is important that they be investigated and that the extent to which they dominate the flowfield be known. Thus, many recent studies have focused on the computation of such flowfields around complex geometries. Although these studies are necessary and valuable, the complexity of the physical processes and numerical solution introduce much uncertainty. The processes of molecular transport, chemical kinetics, and radiative heating must be sufficiently understood and modeled. In addition, numerical issues such as grid convergence and temporal accuracy must also be considered. Moreover, because of the amount of computer time required, these studies are generally performed at only a few design points in the vehicle trajectory.

Received Oct. 14, 1991; accepted for publication Feb. 21, 1992.

*DOD Graduate Fellow, Department of Aerospace Engineering. Student Member AIAA.

†Professor, Department of Aerospace Engineering. Fellow AIAA.

To focus on the validity of various kinetic models currently available, a simple gas dynamic model is used here, namely, the nonequilibrium chemically reacting flowfield downstream of normal shock waves. This flow has been calculated for freestream Mach numbers ranging from $M = 25$ to 58 at altitudes between 61 and 91 km.[2] Data pertaining to the case of $M = 34$ at 61 km altitude are presented herein. This data point is selected because of the high temperatures occurring immediately behind the shock wave, which give rise to significant electronic energy contribution. An 11-species air model is used for the present calculation. Additionally, it is assumed that all internal energy modes of the gaseous species are in equilibrium with the translational mode. Therefore, only one temperature is needed to characterize the energy of the system, and all of the expressions for the energy modes can be obtained directly from statistical thermodynamics.[3,4] Note that the freestream conditions selected for this work are fairly close to proposed scenarios of Earth reentry of a manned Mars mission aerobrake. However, the altitude is approximately 10 km lower to maintain local thermodynamic equilibrium. Further, since the flow is one dimensional, the governing equations reduce to a set of first-order, nonlinear ordinary differential equations. These equations, which can be stiff due to the chemistry, are integrated in the downstream direction by specialized integration packages found in standard math libraries.

The requirement of including equilibrium electronic energy in the evaluation of the enthalpy is first examined. For a mixture, the enthalpy per unit mass can be expressed as

$$h = \sum_{i=1}^{N_s} c_i h_i \tag{1}$$

where

$$h_i = e_i + RT \tag{2}$$

and the index i refers to 1 of the 11 chemical species contained in the mixture. The internal energy for diatomic molecules is composed of four separate modes of energy plus the effective zero point energy that is given by the heat of formation at absolute zero:

$$e_i = \frac{3}{2}RT + RT + \frac{h\nu_i/kT}{e^{h\nu_i/kT} - 1}RT$$

$$+ \left(\frac{\sum(e_n/kT)g_n e^{-e_n/kT}}{\sum g_n e^{-e_n/kT}}\right)_i RT + (\Delta h_f)_i^0 \tag{3}$$

For atomic species, only the translational and electronic modes of energy are present along with the heat of formation. Thus the internal energy is given by Eq. (4):

$$e_i = \frac{3}{2}RT + \left(\frac{\sum(e_n/kT)g_n e^{-e_n/kT}}{\sum g_n e^{-e_n/kT}}\right)_i RT + (\Delta h_f)_i^0 \tag{4}$$

In both cases, e_n is the energy per particle of the nth electronic level. For low-temperature applications, only the translational and rotational modes are excited. For temperatures above approximately 800 K, the contribution of the vibrational energy to the total energy becomes important. The current question is, at what temperature does the electronic energy become significant?

To answer the present question, calculations were made with and without the equilibrium electronic energy using the same kinetic mechanism. In Fig. 1, the resulting temperature distribution is plotted vs distance downstream from the shock wave. Note the abscissa is plotted in logarithmic scale. For both of these curves, the Dunn and Kang kinetic model was used; however, for the solid curve the electronic energy is not included, whereas for the dashed curve, it was included. Clearly, the significant contribution of the electronic energy is in the reduction of temperatures in that portion of the reaction zone where the temperatures are between 20,000 and 52,000 K. In this region the difference in temperature predictions is roughly 2000 K. Far downstream, however, where the gas temperatures are much cooler, approximately 12,000 K, there are negligible differences in the temperature prediction.

Since the chemical reaction rates are exponential functions of temperature, one might ask how this difference of temperature in the reaction zone affects the species mass fractions. In Fig. 2, a comparison of the mass fraction profiles for the neutral molecular species is given. Note that as the flow approaches equilibrium, in the downstream portion of the relaxation zone, the concentrations of these species are noticeably greater for the case where the electronic energy has been included. Although this is consistent with the preceding result, in that including the electronic energy makes less energy available for dissociation, it is interesting that the effects on mass fractions lag behind those that occur for the temperature. This delay is present in the mass fraction profiles for all species in the mixture.

Comparisons of the predictions made by several popular kinetic mechanisms were also explored in this study. In particular, the flowfield obtained from the Dunn and Kang rate mechanism[5] was compared with that obtained from both Park's 1987 mechanism[6] and the updated 1991 model.[7,8] The Dunn and Kang model was derived specifically as a one-temperature model. Rate constants for both the forward and

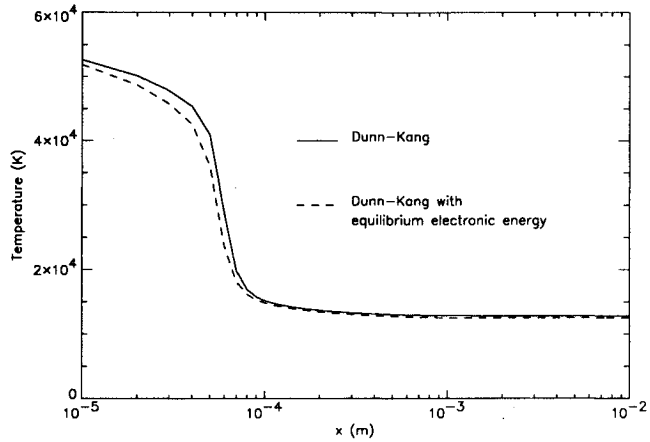

Fig. 1 Comparison of temperature distribution behind a $M = 33.70$, $h = 60.96$ normal shock wave for calculations containing electronic energy contributions.

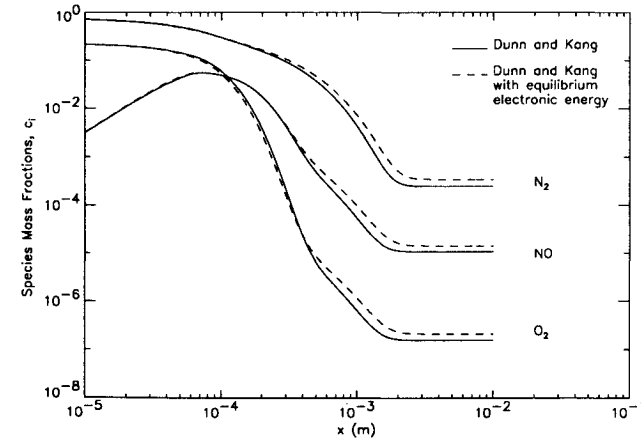

Fig. 2 Comparison of species mass fractions for the neutral molecular species behind a $M = 33.70$, $h = 60.96$ normal shock wave for calculations containing electronic energy contributions.

backward reactions are given in modified Arrhenius form. In contrast, the Park models were modified for thermodynamic nonequilibrium and are commonly referred to as "two-temperature" models. In this study, the Park models are used for thermodynamic equilibrium by assuming that the translational and vibrational temperatures are equivalent. The forward rate constants are again given by the Arrhenius equations. The backward rates, however, are obtained from a curve fit for the equilibrium constants using the well-known relation

$$k_b = \frac{k_f}{K_c} \tag{5}$$

Additionally, calculations were performed with a hybrid model that combines the Dunn and Kang forward rates with the backward rates obtained from Eq. (5) and the curve fits of Gupta et al.[9] for the equilibrium constants. Those fits were determined using 18 data points between 500 and 60,000 K and are more accurate than Park's fits at temperatures above 12,000 K.

Typical results of these comparisons are summarized in Figs. 3 and 4. In Fig. 3, the temperature distribution downstream from the normal shock wave is given as calculated by the four different models that include both of Parks,[6,8] the Dunn and Kang model, and the hybrid Dunn-Kang/Gupta mechanism. The largest discrepancy in the prediction of the relaxation zone occurs between the Park[6] and the Dunn and Kang models. The newer models, Park[8] and the hybrid model, tend to bridge the gap between the extreme predictions of the relaxation zone location. Note that there is very good agreement in the equilibrium value of the predicted temperatures

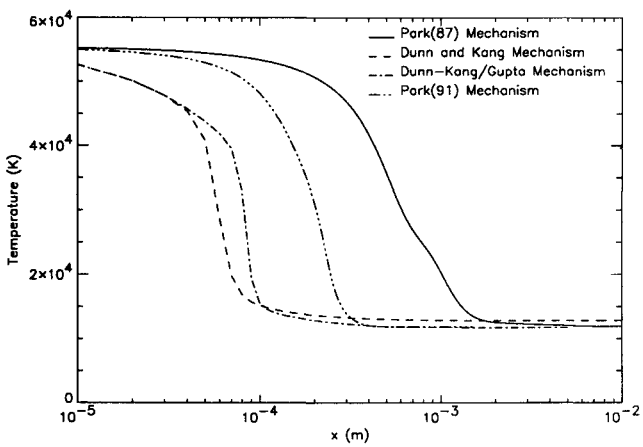

Fig. 3 Comparison of temperature distribution behind a $M = 33.70$, $h = 60.96$ normal shock wave for various kinetic models.

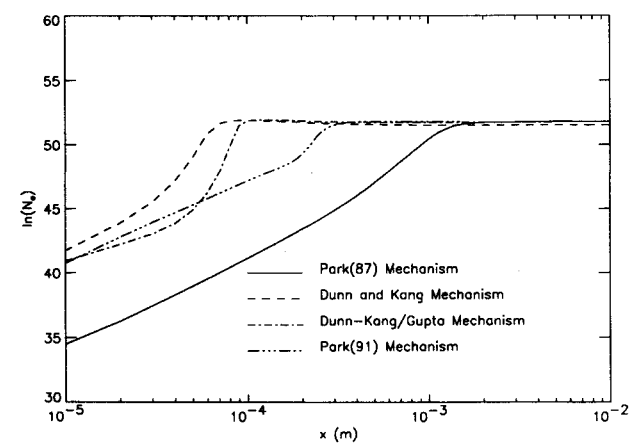

Fig. 4 Comparison of the electron number density behind a $M = 33.70$, $h = 60.96$ normal shock wave for various kinetic models.

downstream of the normal shock wave as predicted by the Park[8] and Dunn-Kang/Gupta mechanisms. This is probably the result of the improved curve fits for the equilibrium constants that were employed in these newer models. In Fig. 4, the logarithm of the electron number density is plotted vs distance downstream of the shock wave. Again, it is particularly evident that the Dunn and Kang model predicts the quickest reaction rate with the electron number density reaching a plateau more than one millimeter ahead of the location as predicted by Park.[6] As with the temperature profiles, the relaxation zones for the Park[8] and hybrid models are located between the two extremes. Thus the use of these newer models reduces the discrepancy in the flowfield predictions. However, the reader is cautioned that there may be some question as to the validity of the hybrid model. In particular, there is some current conjecture as to the validity of mixing and matching parts of reaction mechanisms. Finally, the purpose of the present work is to examine the discrepancy between various kinetic models; no conclusion can be made as to which model is the most correct without having some definitive experimental data with which to compare. Such data are lacking at present.

References

[1]Mitcheltree, R. A., "A Parametric Study of Dissociation and Ionization Models at 12 km/s" AIAA Paper 91-1368, June 1990.

[2]Weber, Y., and Anderson, J. D., Jr., "A Comparison of Chemical Kinetic Rate Mechanisms for High Temperature Air, Including Electronic Energy," Univ. of Maryland, UM-AERO-40, College Park, MD, 1991.

[3]Vincenti, W. G., and Kruger, C. H., *Introduction to Physical Gas Dynamics*, Wiley, New York, 1965, pp. 86–151.

[4]Anderson, J. D., Jr., *Hypersonic and High Temperature Gas Dynamics*, McGraw-Hill, New York, 1988, pp. 413–467.

[5]Dunn, M. G., and Kang, S. W., "Theoretical and Experimental Studies of Reentry Plasmas," NASA CR-2232, April 1973.

[6]Park, C., "Assessment of Two-Temperature Kinetic Model for Ionizing Air," AIAA Paper 87-1574, June 1987.

[7]Park, C., *Nonequilibrium Hypersonic Aerothermodynamics*, Wiley, New York, 1990.

[8]Park, C., "Chemical-Kinetic Problems of Future NASA Missions," AIAA Paper 91-0464, Jan. 1991.

[9]Gupta, R. N., Yos, J. M., Thompson, R. A., and Lee, K., "A Review of Reaction Rates and Thermodynamic and Transport Properties for an 11-Species Air Model for Chemical and Thermal Nonequilibrium Calculations to 30,000 K," NASA RP-1232, Aug. 1990.

Preferential Thermal and Multicomponent Species Transport Effects in Strained Diffusion Flames

J. C. Hermanson* and A. Vranos†
United Technologies Research Center, East Hartford, Connecticut 06108

Introduction

THE study of the structure of laminar diffusion flames is relevant to a number of combustion problems, such as flat flames established between opposing reactant jets and curved flames stabilized above porous spheres or cylinders.[1] In addition, laminar flame elements have been incorporated in

Received Sept. 16, 1991; revision received May 12, 1992; accepted for publication May 13, 1992.

*Research Scientist, Advanced Propulsion, Power, and Flight Systems, Mail Stop 29. Senior Member AIAA.

†Consulting Scientist, Environmental Sciences, Industrial Systems, and Technology, Mail Stop 30. Member AIAA.